ELSEVIER

Journal of Power Sources 105 (2002) 182–188

JOURNAL OF POWER SOURCES

www.elsevier.com/locate/jpowsour

New materials for supercapacitors

M. Wohlfahrt-Mehrens*, J. Schenk, P.M. Wilde[1], E. Abdelmula[2], P. Axmann, J. Garche

EC Energy Storage and Conversion Division, Center for Solar and Hydrogen Research Baden Wuerttemberg (ZSW) Helmholtzstrasse 8, D-89081 Ulm, Germany

Abstract

Ruthenates based on $SrRuO_3$ perovskite exhibit pseudocapacitance behavior. Replacing up to 20 mol% Sr by La leads to an increase of the specific capacity. The stability window of ruthenates is strongly dependent on B-site cations. Fe or Co substitution reduces the stability of the electrolyte whereas 20 mol% doping by Mn on the B-site increases the capacity without reducing the potential window. A capacitance up to 270 F/g was obtained by optimizing composition and preparation route.

Cobalt or aluminum mixed hydroxides/oxyhydroxides also seems to have the potential for high pseudocapacitance behavior and exhibit capacitance up to 360 F/g, but the potential window is very limited.

Keywords: Supercapacitor; Perovskite; Strontium ruthenate; Cobalt/aluminum hydroxide

1. Introduction

Among the oxide materials for application in supercapacitors ruthenium and iridium oxides have achieved much attention [1–7]. Ruthenium oxides are easy to prepare, e.g. thermal decomposition of $RuCl_3 \cdot H_2O$ onto titanium or tantalum foil [5], show metallic conductivity, have a high double layer and pseudocapacitance and are stable in aqueous acid and alkaline electrolytes. The capacitance sensitively depends on the method of preparation. Up to 500 F/g [5] or 720 F/g [6] are reported for amorphous water-containing ruthenium oxides. In these amorphous ruthenium oxides the interaction of the proton of the hydroxide group with the constitutional water and the electrolyte is the reason for the very high capacitance.

The disadvantage of RuO_2 is the high cost of raw material. Therefore, in recent years great efforts were undertaken in order to find new and cheaper materials. Different research trends are observable, e.g. nitrides, oxynitrides and carbides [8–10], sol–gel derived Ni_xO/Ni thin film electrodes [11,12] or Ti–V–WO/Ti electrodes [13].

One possible way to reduce costs is the partial substitution of ruthenium in a wider type of oxide structure. Alkaline earth ruthenates with perovskite structure of the general formula ABO_3 containing ruthenium on the B position have been shown to exhibit pseudocapacitance behavior [14–16]. These materials show metallic conductivity [17] and are stable in aqueous alkaline electrolytes.

Another interesting class of materials is the nickel or cobalt oxyhydroxides. These materials show good electronic conductivity and there exist various structure types containing water in the host structure with high proton mobility.

The aim of this contribution is to review our work on ruthenates with perovskite structure as well as to discuss the influence of dopants. We also present the first results for cobalt/aluminum hydroxides/oxyhydroxides.

2. Experimental

2.1. Synthesis

2.1.1. Perovskites

The perovskites are prepared either by coprecipitation or by a direct pyrolysis route [16]. In the first case stoichiometric metal salt solutions of ruthenium chloride, strontium and other metal nitrates were coprecipitated in 3 M KOH at room temperature. The precipitate was filtered and washed with distilled water until the filtrate was free of chlorine

* Corresponding author. Tel.: +49-731-9530601; fax: +49-731-9530666.
E-mail address: margret.wohlfahrt-mehrens@zsw-bw.de (M. Wohlfahrt-Mehrens).
[1] Present address: SGL Technik GmbH, W.-v.-Siemens-Straße 18, D-86405 Meitingen, Germany
[2] Present address: Dechema, Theodor-Heuss-Allee 25, D-60486 Frankfurt

0378-7753/02/$ – see front matter
PII: S0378-7753(01)00937-5

anions. Subsequent calcination at 500–1000 °C led to pure phase perovskites. The annealing temperature was strongly dependent on the doping elements. Pure $SrRuO_3$ was obtained in the temperature range of about 500–600 °C. For samples containing lanthanum, iron, cobalt and manganese the temperature had to be raised up to 800 °C in order to get single phase materials.

Following a pyrolysis route the precursor was an aqueous solution of ruthenium chloride and strontium nitrate well in excess. This solution was pyrolysed at temperatures about 500 °C. The samples usually contain the desired perovskite and large amounts of water-soluble strontium chloride and its hydrates. After removing these phases by washing with distilled water porous samples of pure perovskites were obtained. In some cases trace amounts of ruthenium dioxide were detectable. It could be shown that RuO_2 prepared under similar conditions exhibits almost no capacitance compared to the perovskites. Therefore, small impurities of RuO_2 were tolerated for electrochemical measurements.

2.1.2. Nickel/cobalt/aluminum hydroxides

Nickel aluminum double layer hydroxides and cobalt or aluminum double layer hydroxides were prepared according to the route given in references [17,18]. Stoichiometric metal nitrate solutions were coprecipitated in 2 M sodium hydroxide solution containing 2 M sodium carbonate at 40 °C. The suspension was stirred at 70 °C for 55 h. The precipitate was separated by centrifugation and carefully washed with distilled water to separate the nitrate. The powder was dried at 70 °C. For some samples the powder was hydrothermal by treated at 130 °C.

2.2. Structural and chemical characterization

Phase composition was determined by X-ray powder diffractometry using a Siemens D5000 machine with a graphite secondary monochromator, Bragg-Brentano focussing and Cu Kα radiation. High temperature XRD measurements were performed in a Buehler S1 chamber attached directly to the goniometer. Chemical analysis was done by ICP analysis. The BET surface area of larger sample batches was determined in a Carlo-Erba Sorptomatic model 1990 using nitrogen adsorption.

2.3. Electrode preparation

In the case of alkaline earth ruthenates electrodes were prepared by painting a slurry of the perovskite powder in an aqueous solution with Triton X-100 (10:1) on one side of nickel foils. The nickel sheets were previously etched in boiling HCl in order to remove oxide layers and to get higher surface areas. To achieve better adherence of the coating layer the electrodes were annealed at 300–400 °C for 2 h in air after painting. The dimensions of the electrodes were 15 mm × 15 mm. Typical amounts of active mass were in the range of 2 mg/cm^2, which was determined by difference weighing before and after coating.

Cobalt/aluminum hydroxides were mixed with 50 wt.% graphite (Heraeus, 40–100 mm, 99% 009075) and 2 wt.% binder (Hostaflon 2025, Hoechst) and pressed on nickel grid (4–5 t). The loading of the electrode was typically in the range of 20 mg/cm^2.

2.4. Electrochemical characterization

All electrochemical measurements were done in a three electrode arrangement. A platinum foil was used as reference electrode. All potentials are referred to Hg/HgO reference electrode in the same electrolyte. All measurements were carried out in 6 M KOH electrolyte. Cyclic voltammogramms at various scan rates varying from 1–1000 mV/s were performed using an EG&G PAR model 273 potentiostat, controlled by a microcomputer.

Specific capacitance was calculated by integrating the current of a cyclic voltammogram half cycle and relating the charge to the voltage range and the weight of active mass. The current densities in the diagrams are given with respect to the active mass loading rather than to the geometric area. The data of cyclic voltammograms of different materials can be compared more easily and do not depend on electrode loading.

3. Results and discussion

3.1. Doped strontium ruthenates

Fig. 1 shows the cyclic voltammogram of pure $SrRuO_3$ prepared by a coprecipitation route and calcination at 800 °C. The shape of the cyclic voltammogram is nearly rectangular which is characteristic of electrochemical capacitors. The stability window is about 1.2 V. The differential capacity calculated from the cyclic voltammogram is about 8 F/g. Some weak oxidation and reduction peaks are observed in the potential range between 0.15 and 0.25 V

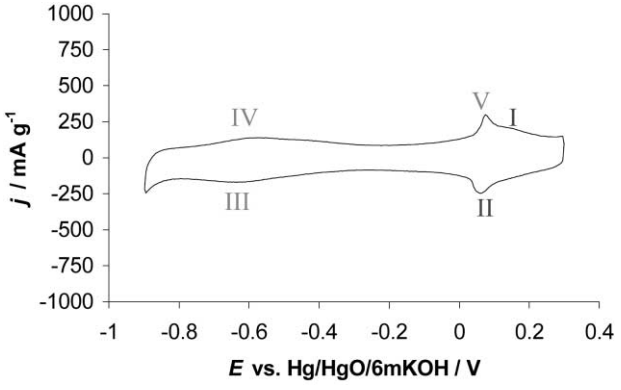

Fig. 1. Cyclic voltammogramm of $SrRuO_3$, synthesized by coprecipitation annealed at 800 °C, scan rate 20 mV/s.

versus Hg/HgO. The redox reaction in regions I and II can be explained by a Ru(IV) ↔ Ru(V) reaction [15,16].

I $SrRuO_3 + OH^- \rightarrow SrRuO_3OH + e^-$ (II)

II $SrRuO_3 + H_2O + e^- \rightarrow SrRuO_2OH + OH^-$

III Partial removal of bulk protons (II)

IV Complete deprotonation

Normally only the surface layers of the ruthenium oxides are involved in these redox reactions. The reasoning here is that protons are necessary in the redox reaction. For keeping the charge balance protons have to enter (reduction process) or to leave (oxidation process) the host structure. On the other hand, the oxidation of Ru(IV) to Ru(V) or Ru(VI) leads to an excess of positive charge. Therefore, additional anions have to enter the host structure-possibly OH^- ions from the electrolyte. Both proton and hydroxide diffusion require a certain free volume in the host lattice and/or lattice defects within the structure. The free volume of the perovskite structure is determined by the ionic radii of cations and anions.

In order to improve capacity properties the influences of substitution of A and B cations were investigated and various preparation methods were applied. The aim of the work was increasing the capacity and reducing the amount of ruthenium by

- increase of proton mobility in the perovskite structure;
- building in of other redox components;
- increase of surface by preparation process.

3.1.1. A-site doped strontium ruthenate

If strontium is partly replaced by lanthanum the upper voltage region is nearly unchanged (Fig. 2).

In contrast to pure $SrRuO_3$ a broad redox couple occurs at potentials in the region between −600 and −800 mV versus Hg/HgO resulting in higher specific capacities. Due to the smaller ionic radius of La^{3+} compared to Sr^{2+} the free volume in the lattice structure will be reduced in lanthanum-doped $SrRuO_3$. On the other hand partial substitution of Sr^{2+} by La^{3+} induces a certain amount of ruthenium in the trivalent state due to charge neutrality. This fact explains the shift of the redox potential in the cyclic voltammogramm. Also the stability range is affected by lanthanum dopants. For $Sr_{0.8}La_{0.2}$ RuO_3 it is 0.1 V larger compared to undoped $SrRuO_3$.

3.1.2. B-site doped strontium ruthenate

Figs. 3 and 4 show the steady-state cyclic voltammograms for various compositions of cobalt-and iron-doped strontium ruthenates. It is assumed that iron and cobalt are incorporated in the trivalent state. The cyclic voltammogramms show no significant difference in redox behavior compared to pure $SrRuO_3$. The increasing amount of cobalt and iron does not effect the specific capacitance. But a decrease of the stability window is observed with increasing amount of cobalt and iron. This is expressed by the onset of hydrogen evolution, which is shifted towards more positive potentials for higher dopant concentrations. Even small amounts of cobalt or lead to a significant decrease of the potential window, whereas the effects are not so large for iron-doped materials.

In the case of manganese-doped strontium ruthenate an additional redox activity is observed at potentials about −400 mV versus Hg/HgO (Fig. 5). This behavior can possibly be explained by the incorporation of manganese in the trivalent state. Mn(III) as a Jahn–Teller-ion may lead to a distortion of the host lattice and induce defects in the structure resulting in an enhancement of proton mobility. The reason for the nonlinear correlation between the increase in capacitance and the corresponding manganese content is not known at the moment. Further experiments are also needed to understand the influences which determine the stability window of the ruthenates.

3.1.3. Influence of preparation route

The capacity of the strontium ruthenates can also be enhanced by optimised preparation routes. Fig. 6 shows the cyclic voltammogramm of $Sr_{0.8}La_{0.2}Ru_{0.8}Mn_{0.2}O_3$ pre-

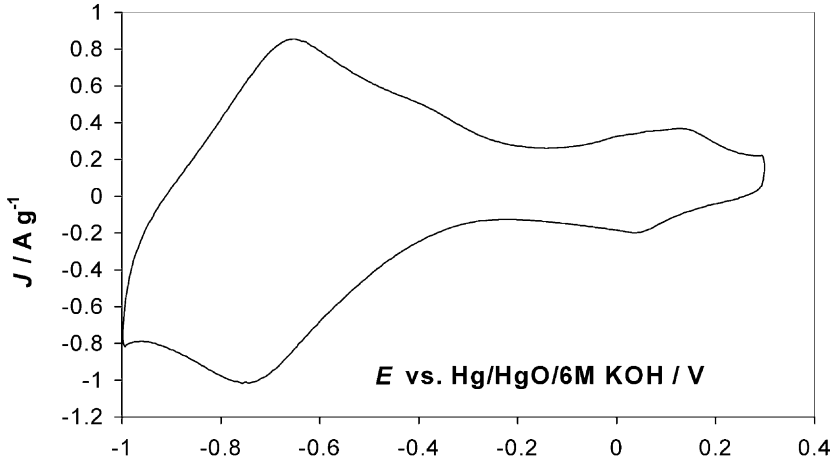

Fig. 2. Cyclic voltammogramm of $Sr_{0.8}La_{0.2}RuO_3$ synthesized by coprecipitation annealed at 800 °C, scan rate 20 mV/s.

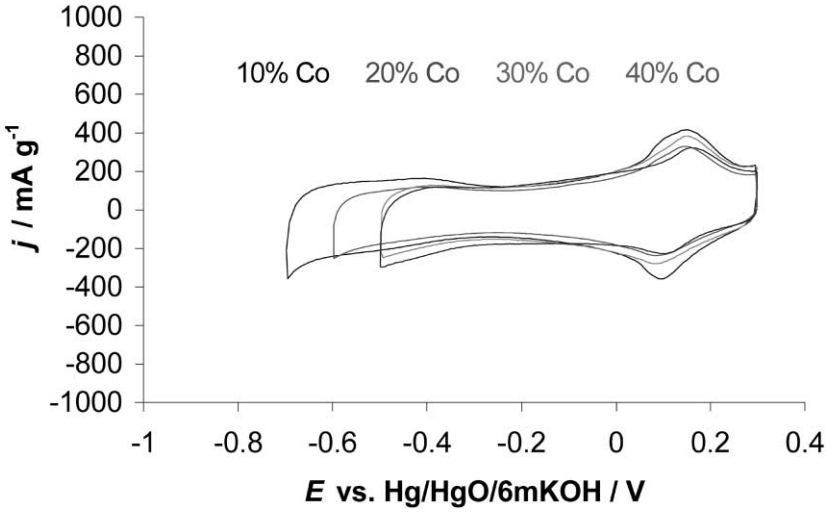

Fig. 3. Cyclic voltammogramm of various cobalt-doped strontium ruthenates $SrRu_{1-x}Co_xO_3$ with $x = 0.1$, 0.2, 0.3 and 0.4 synthesized by coprecipitation annealed at 800 °C, scan rate 20 mV/s.

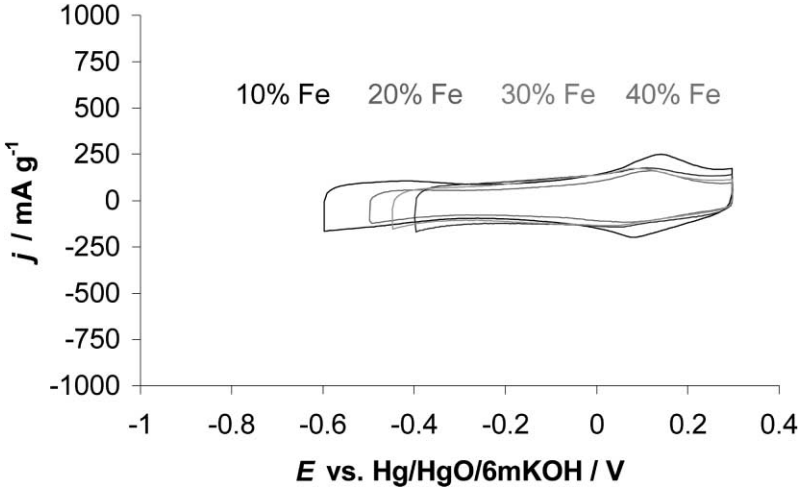

Fig. 4. Cyclic voltammogramm of various iron-doped strontium ruthenates $SrRu_{1-x}Fe_xO_3$ with $x = 0.1$, 0.2, 0.3 and 0.4 synthesized by coprecipitation annealed at 800 °C, scan rate 20 mV/s.

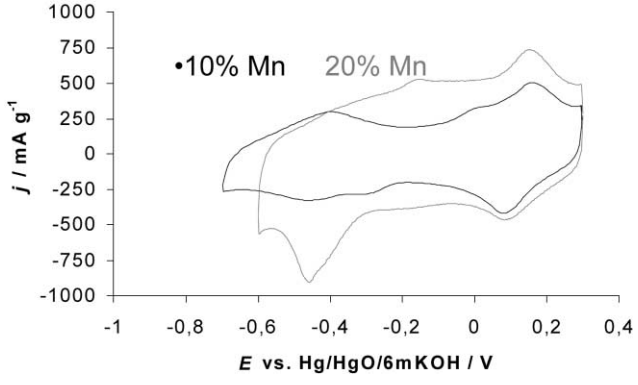

Fig. 5. Cyclic voltammogramm of various manganese-doped strontium ruthenates $SrRu_{1-x}Mn_xO_3$ with $x = 0.1$, 0.2, synthesized by coprecipitation annealed at 800 °C, scan rate 20 mV/s.

pared by a pyrolysis route at 500 °C. The current density is much higher than for the corresponding samples prepared by coprecipitation. The larger specific capacity is due to the higher surface area and therefore an increased number of reachable active sites. Bulk utilization seems also to be enhanced by the high defect structure due to rapid temperature changes during the preparation process. Table 1 gives a summary of preparation and dopants. By using optimum synthesis conditions capacitance values up to 270 F/g were reached.

3.1.4. Nickel/cobalt/aluminum hydroxides

Nickel aluminum and cobalt or aluminum double layer hydroxides were prepared using the coprecipitation route described above. The nickel/aluminum, respectively cobalt/aluminum ratio was 2:1. All materials show the typical

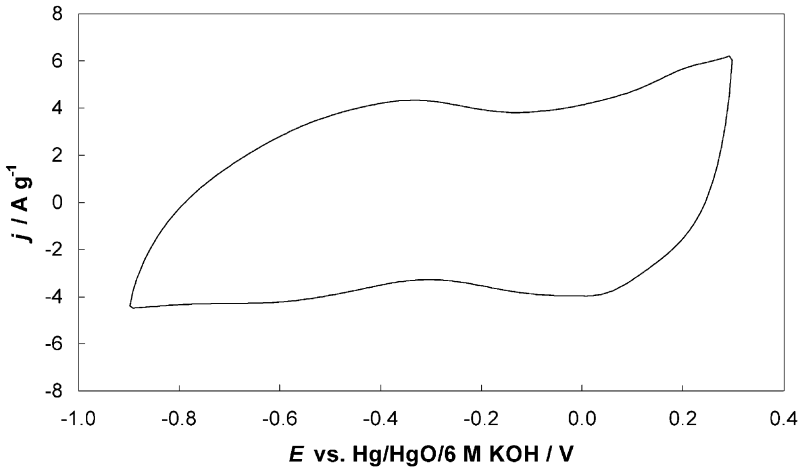

Fig. 6. Cyclic voltammogramm of $SrRuO_3$ prepared by pyrolysis route at 500 °C.

Table 1
Specific capacitances of pure and doped perovskite materials prepared by different techniques in comparison to RuO_2

Material	Synthesis	[Ru] (wt.%)	C (F/g)	C (F/g_{Ru})
$SrRuO_3$	Coprecipitated 800 °C	43	8	18.75
RuO_2	Coprecipitated 800 °C	76	20	26.34
$La_{0.2}Sr_{0.8}RuO_3$	Coprecipitated 800 °C	41	21	51.25
$SrMn_{0.2}Ru_{0.8}O_3$	Coprecipitated 800 °C	36	28	78.77
$La_{0.2}Sr_{0.8}Mn_{0.2}Ru_{0.8}O_3$	Pyrolysis 500 °C	34	160	470.40
$SrRuO_3$	Optimizing pyrolysis 500 °C	43	270	632.31
$RuO_2{\cdot}2H_2O$	Sol–gel	60	485	811.53
$RuO_2{\cdot}2H_2O$	Sol–gel	60	720	1204.75

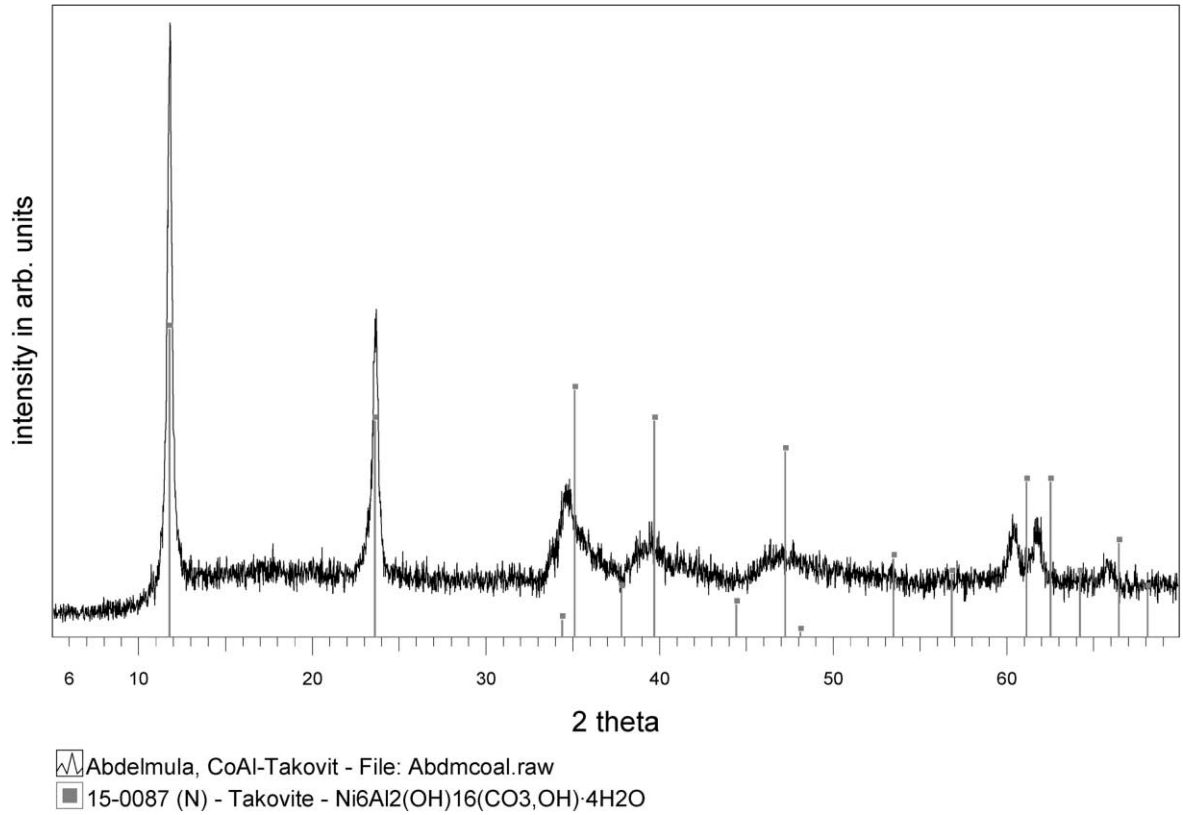

Fig. 7. XRD pattern of $[Co_{1-x}Al_x(OH)_2]^{x+}$ $[CO_3^{2-}]_{x/2}{\cdot}[H_2O]_z$ with $x = 0.33$.

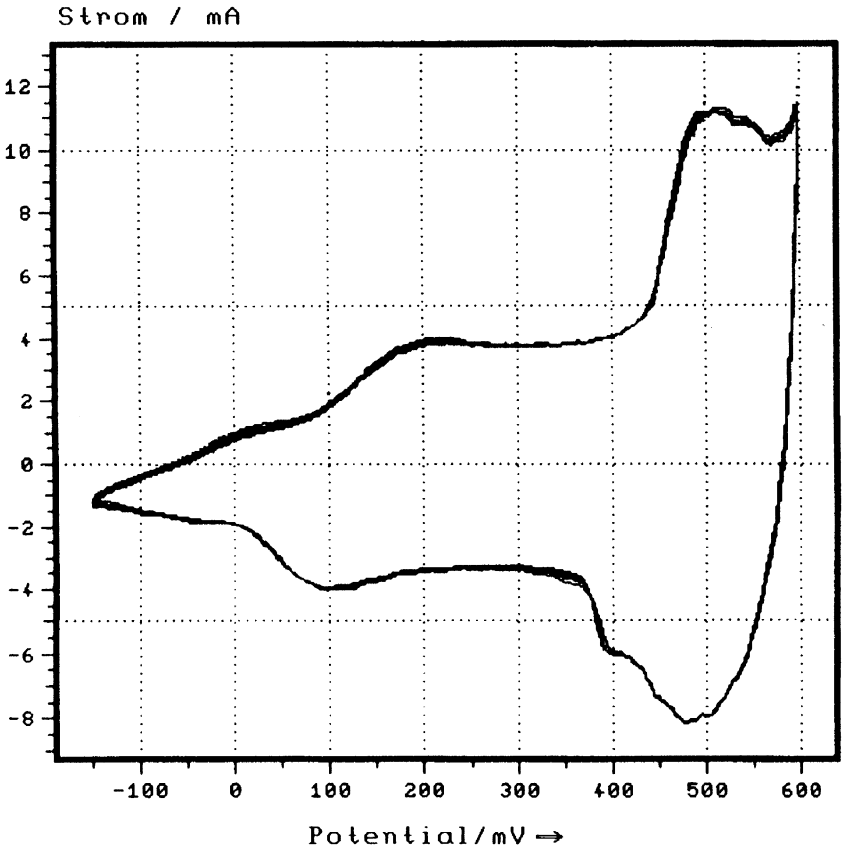

Fig. 8. Cyclic voltammogramm of $[Co_{1-x}Al_x(OH)_2]^{x+}[CO_3^{2-}]_{x/2}\cdot[H_2O]_z$ with $x = 0.33$ prepared by coprecipitation method in 6 M KOH, scan rate 1 mV/s.

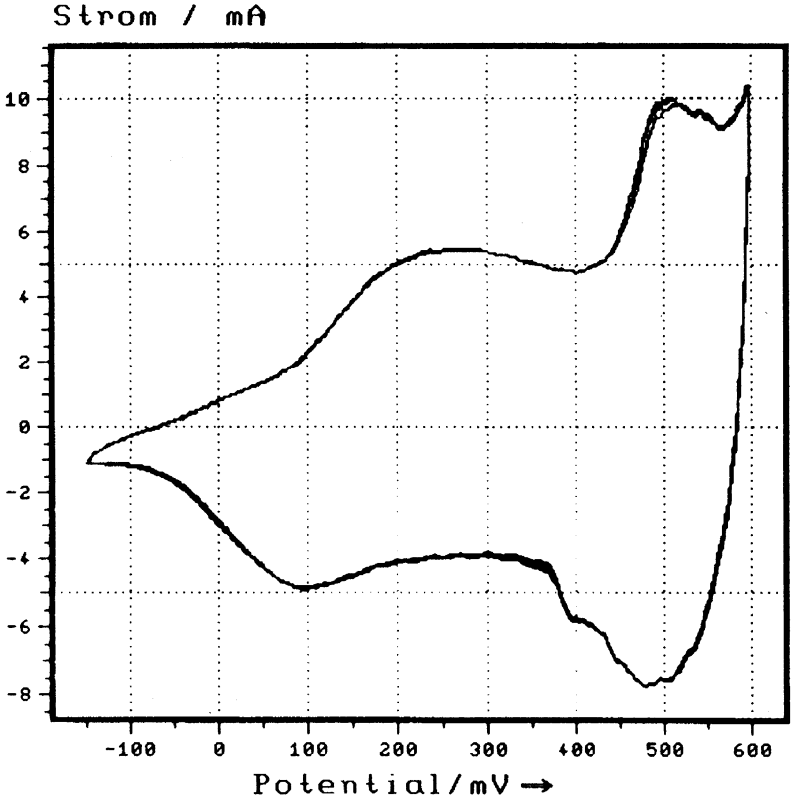

Fig. 9. Cyclic voltammogramm of $[Co_{1-x}Al_x(OH)_2]^{x+}[CO_3^{2-}]_{x/2}\cdot[H_2O]_z$ with $x = 0.33$ prepared by coprecipitation and additional hydrothermal treatment in 6 M KOH, scan rate 1 mV/s.

Table 2
Specific capacitances of nickel and cobalt hydroxides/oxyhydroxides

Material	Synthesis	C (F/g)	ΔU (mV)
Ni/Al hydroxide	Coprecipitaion	12	90
Ni/Al hydroxide	Hydrothermal	12	230
Ni/Al/V	Coprecipitation	30	100
Co/Al hydroxide	Coprecipitation	300	400
Co/Al hydroxide	Hydrothermal	360	420

diffraction pattern of double layer hydroxides. Fig. 7 gives the XRD pattern of coprecipitated $[Co_{1-x}Al_x(OH)_2]^{x+}$-$[CO_3{}^{2-}]_{x/2}\cdot[H_2O]_z$ with $x = 0.33$. The cyclic voltammogramm of $[Co_{1-x}Al_x(OH)_2]^{x+}[CO_3{}^{2-}]_{x/2}\cdot[H_2O]_z$ with $x = 0.33$ is given in Fig. 8. In the potential range of 150–570 mV versus Hg/HgO the sample shows a pseudocapacitance behavior. The redox couple of Co^{2+}/Co^{3+} occurs around 500 mV versus Hg/HgO. A capacitance of about 360 F/g was obtained with a hydrothermal-treated cobalt or aluminum double layer hydroxide (Fig. 9). For practical applications the potential window with about 400 mV is very low. Table 2 gives a summary of the synthesis conditions and capacitance behavior of various samples. Further work about the interactions between chemical composition, lattice structure and electrochemical behavior is in progress.

4. Conclusions

The pseudocapacitance of earth alkali ruthenates with perovskite structure could be increased by improving the synthesis conditions and the composition by doping on A-sites and B-sites. The redox capacity depends on the mobility of protons in the host lattice. The free lattice volume can be influenced either by foreign doping metals or by inducing defects in the lattice. The best results were obtained by using $La_{0.2}Sr_{0.8}RuO_3$ prepared via a pyrolysis route. The different storage mechanisms of doped materials are not fully understood at the present time. Further work is necessary to explain the differences between manganese and cobalt-doped materials. Cobalt or aluminum double layer hydroxides also show good capacitance behavior. The potential window is rather limited.

Acknowledgements

The German ministry of science, education and research (BMBF) is gratefully acknowledged for supporting a part of this work under Contract no. 03N 3007 E7 in cooperation with Dornier GmbH, Friedrichshafen, Germany.

References

[1] S. Trasatti, G. Buzzanca, J. Electroanal. Chem. 29 (Suppl. 1) (1971).
[2] D. Galizioli, F. Tantardini, S. Trasatti, J. Appl. Electrochem. 4 (1974) 57.
[3] B.E. Conway, J. Electrochem. Soc. 138 (1991) 1539.
[4] B.E. Conway, Electrochemical Supercapacitors, Plenum Press, New York, 1999, p. 259.
[5] M. Goodwin, in: Proceedings of the 6th International Seminar on Double Layer Capacitors and Similar Energy Storage Devices, Deerfield Beach, FL, USA, 1996.
[6] S. Trasatti, P. Kurzweil, Plat. Met. Rev. 38 (2) (1994) 46.
[7] J.E. Oxley, in: Proceedings of 34th International Power Sources Symposium, Cherry Hill, NJ, USA, 25–28 June 1990.
[8] W.D. Ryden, A.W. Lawson, C.C. Sartain, Phys. Lett. 26A (1968) 209.
[9] P. Kurzweil, O. Schmid, A. Löffler, A. Koch, in: Proceedings of the 7th International Seminar on Double Layer Capacitors and Similar Energy Storage Devices, Deerfield Beach, FL, USA, 1997.
[10] J.P. Zeng, T.R. Jow, J. Electrochem. Soc. 142 (1) (1995) L6.
[11] M. Goodwin, in: Proceedings of the 6th International Seminar on Double Layer Capacitors and Similar Energy Storage Devices, Deerfield Beach, FL, USA, 1996.
[12] M. Wixom, in: Proceedings of the 5th International Seminar on Double Layer Capacitors and Similar Energy Storage Devices, Boca Rota, FL, USA, 1995.
[13] C.Z. Deng, R.A.J. Pynenburg, K.C. Tsai, J. Electrochem. Soc. 145 (1998) L61.
[14] K.C. Liu, M.A. Anderson, in: Electrochemical capacitors II, F.M. Delnick, D. Ingersoll, X. Andrieu, K. Naoi (Eds.), PV96-25, The Electrochemical Society Series, Pennington, NJ, 1997, p. 68.
[15] V. Srinivasan, J.W. Weidner, J. Electrochem. Soc. 144 (1997).
[16] Y. Takasu, S. Mizutani, M. Kumagai, S. Sawaguchi, Y. Murakami, Electrochem. Solid-State Lett. 2 (1) (1999) 1.
[17] R. Oesten, T. Guther, J. Garche, in: Proceedings of the 6th International Seminar on Double Layer Capacitors and Similar Energy Storage Devices, Deerfield Beach, FL, USA, 1996.
[18] T.J. Guther, R. Oesten, J. Garche, Electrochemical capacitors II, in: F.M. Delnick, D. Ingersoll, X. Andrieu, K. Naoi (Eds.), The Electrochemical Society Proceedings Series, Vol. PV, Pennington, NJ, USA, 1997, p. 16.